Electronic Supplementary Material (ESI) for Chemical Science.

Supporting Information

Unexpected High Selectivity for Acetate Formation from CO_2 Reduction with Copper Based 2D Hybrid Catalysts at Ultralow Potentials

Rongming Cai,[a] Mingzi Sun,[b] Jiazheng Ren,[a] Min Ju,[a] Xia Long,*[a] Bolong Huang,*[b] and Shihe Yang*[a]

[a] R. Cai, Dr. J. Ren, M, Ju, Prof. X. Long, Prof. S. Yang

Guangdong Provincial Key Lab of Nano-Micro Material Research, School of Chemical Biology and Biotechnology, Shenzhen Graduate School, Peking University, Shenzhen 518055 (China)

E-mail: xialong@pku.edu.cn, chsyang@pku.edu.cn

[b] M. Sun, Prof. B. Huang

Department of Applied Biology and Chemical Technology,The Hong Kong Polytechnic University,Hung Hom, Kowloon, Hong Kong SAR (China)

E-mail: bhuang@polyu.edu.hk

Experimental Details

1. Chemicals

Copper(II) nitrate trihydrate (AR,99%, Macklin), Potassium fluoride (99%, Energy-chemical), Hexamethylenetetramine (99+%, Alfa Aesar), Potassium hydroxide for sample preparation(99%, Aladdin), Potassium hydroxide used for electrolyte(>90%, General-reagent), Ethanol (AR, Sinopharm), Water (18.25 MΩ), Carbon paper(Gaossunion), Nafion(5 wt.% in mixture of lower aliphatic alcohols and water, Sigma-Aldrich). Dimethyl sulfoxide (>99.9%, Aladdin), Deuterium oxide (99.9 atom % D, Macklin). All chemicals in this work were purchased commercially and used without further purification.

2. Synthesis of Cu(OH)F precursor

Cu(OH)F was synthesized via hydrothermal method.[1] Typically, 0.46g of copper nitrate trihydrate and 0.21g of HMT were dissolved in 15ml of deionized water with stirring at room temperature for 10 minutes, then 0.44g of KF was added with further stirring for 15 minutes. The mixed solution was poured into a stainless steel autoclave and sealed. Then it was heated to 95 °C at a rate of 5 °C · min^{-1} and kept for 2 hours. The autoclave was cooled to room temperature naturally, the reaction product was centrifuged and cleaned 5 times with deionized water, finally washed with ethanol and dried at 60 °C in a vacuum oven for one night. The green product was obtained.

3. Synthesis of $Cu(OH)_2$ precursor

$Cu(OH)_2$ was synthesized by chemical co-precipitation method. 1.21 g of copper nitrate trihydrate was dissolved in 15 ml of deionized water with sonication for 5 minutes, 5 ml of 1 M KOH solution was poured into above solution with vigorously stirring. After reaction, the mixture was transferred to a bigger beaker with 1 L of deionized water to make it settle, then the supernatant was decanted to remove undesired ions. Finally, the product was transferred to a 50 ml of centrifugal tube, washed 6 times with deionized water and ethanol, dried at 60 °C in a vacuum oven for one night.

4. KOH-treated Cu(OH)F

The F-doped $Cu(OH)_2$ was topologically transformed from precursor Cu(OH)F in 1 M KOH solution. Specifically, above synthesized Cu(OH)F was dipped in 1 M KOH for 1 hour. The color was totally changed from green to black, the F-doped $Cu(OH)_2$ was obtained.

5. Synthesis of Cu/Cu_xOF, Cu/Cu_xO and Cu-(111)

Cu/Cu_xOF, Cu/Cu_xO and Cu-(111) were obtained from precursors of Cu(OH)F, KOH-treated Cu(OH)F and $Cu(OH)_2$, respectively, via linear sweep voltammetry (LSV) (generated by CHI 760e). First, adding 2 mg of precursor powders and 16 μl of 5% Nafion solution to 400 ul of ethanol, after sonication for 1 hour, the mixture was drop coated on a 1 cm^{-2} of carbon paper to fabricate a working electrode. Then, the electrochemical transformation process was performed in a flowcell under the same condition as for the alkaline CO_2RR (See details in the part of electrochemical test), The LSV curve (0 ~ -0.9 V vs.RHE, 5 mV/s) was collected immediately when the working electrode contacted the 1 M KOH electrolyte. And the final catalysts of Cu/Cu_xOF, Cu/Cu_xO and Cu-(111) were obtained when the LSV curves were stable (~3 curves). For better a understanding, the basic information of these three catalyts were summarized below:

Catalyst name	Precursor	Formation method	Atomic ratio of F (%)	Morphology
Cu/Cu_xOF	Cu(OH)F	Electrochemical	~5.92%	2D hetereostructure
Cu/Cu_xO	KOH-treated Cu(OH)F		~0.18%	2D hetereostructure
Cu-(111)	$Cu(OH)_2$		0	2D nanoplates

6. Morphology characterizations

Scanning electron microscope (SEM) measurements were performed on a field emission SEM (ZEISS SUPRA®55). The transmission electron microscopy (TEM), high resolution TEM (HRTEM) and TEM energy dispersive X-ray spectrometer (TEM-EDX) were performed on a JEM3200FS field emission source transmission electron microscope equipped with energy dispersive X-ray spectrometer. The ethanol solvent containing catalyst powders were sonicated for two hours, then dropped onto the molybdenum grid for TEM, HRTEM and TEM-EDX characterization. Atomic force microscopy (AFM) samples were prepared by drop drying the catalyst suspensions onto a large silicon wafer and the height images and phase images were recorded on a Brucker Dimension Icon using tapping mode.

7. Structure characterizations

Powder X-ray diffraction (XRD) patterns were recorded using a Rigaku D/Max-2200 PC diffractometer in the diffraction angle range 2-theta from 5–80° with Cu Kα radiation (λ = 1.5418 Å) at 40 kV, 40 mA. X-ray photoelectron spectroscopy (XPS) measurements and Auger electron spectroscopy (AES) measurements were carried out on an ESCALAB 250Xi (Thermo Fisher), a monochromatic aluminium Kα radiation (1486.6 eV) X-ray source was used. Electron paramagnetic resonance (EPR) measurements were performed with a modulation field of 1 mT and a modulation frequency of 100 kHz on a Magnettech ESR 5000 (Bruker), each run lasted 60 s. The *in situ* electrochemical quartz crystal microbalance with dissipation monitoring (EQCM-D) measurements were carried out on a Q-sense E1 (Biolin scientific). The precursor Cu(OH)F was dispersed in ethanol and sonicated to form the precursor ink. Then the ink was dropped on the electrochemical gold sensors with d~ 0.5 cm as the working electrode. The Ag/AgCl and Pt were acted as the reference and counter electrodes, respectively. The electrolyte was 1 M KOH. The monitoring started after the frequency of the resonator was stable when injected the DI water, which was considered as the baseline and set to 0. After KOH electrolyte was injected into the gold sensor, the cyclic voltammetry scan (0 ~ -0.4 V vs.RHE, 5 mV/s) was applied to the working electrode immediately. As for the investigation on the transformation process of KOH-treated Cu(OH)F, the same steps without applied potentials were conducted.

8. Electrochemical tests

The electrochemical performance of CO_2RR was tested on an electrochemical station (CHI 760e) based on three-electrode system using a flowcell reactor (Gaossunion). In the three-electrode system, a piece of carbon paper (1×1 cm) containing the electrocatalysts served as working electrode (Gas diffusion electrode, GDE) with the loading amount of ~ 2 mg/cm^2, the carbon plate and Hg/HgO (1 M KOH) were employed as counter and reference electrode, respectively. As for the flowcell reactor, an anion exchange membrane (Fuma FAA-PK-130, Gaossunion) was utilized for separating the catholyte chamber and anolyte chamber. The aqueous solution of 1 M KOH was used as electrolyte. During the test of CO_2RR, highly purified CO_2 was continuously flowed on the working electrode with a constant flow rate of 20 S.C.C.M., all obtained polarization curves for CO_2RR were recorded without IR-corrections. CO_2RR was applied with a constant potential ranging from -0.3 V to -0.8 V vs.RHE. The gas products were analyzed on a Gas Chromatography (GC 2014C, SHIMADZU Excellence in Science) equipped with two flame ionization detectors (DFID and SFID) and one thermal conductivity detector (TCD). The content of hydrogen was determined by the TCD, and the content of CO and C_2H_4 were determined by the DFID and the SFID, respectively. The liquid product was measured by 1H-NMR spectra using an AVANCE-III (400 MHz, Bruker) spectrometer, and a certain amount of dimethyl sulfoxide (DMSO) was used as the internal standard for quantitative analysis of liquid products. All the tests were performed at room temperature.

9. Calculation Setup

To investigate the electronic structures and energetic trend, we have selected DFT calculations within CASTEP packages for H-Cu/Cu_xOF hybrid electrocatalysts [7]. To supply an accurate description of the exchange-correlation, we have selected the generalized gradient approximation (GGA) and Perdew-Burke-Ernzerhof (PBE) in this work[8-10]. Meanwhile, the plane-wave basis cutoff energy has been set to 380 eV with an ultrafine quality. We choose the ultrasoft pseudopotentials and the Broyden-Fletcher-Goldfarb-Shannon (BFGS) algorithm to deal with the energy minimizations. Based on the convergence tests, the coarse quality of the k-point set is sufficient to guarantee the calculation efficiency and accuracy[11]. For H-Cu/Cu_xOF hybrid electrocatalysts, small Cu nanoparticles with high index facets have been placed on the Cu_xOF nanoplate. Cu_xOF nanoplate has been cleaved from the (111) surfaces of Cu_2O with five-layer thickness. Then, F atoms have been introduced to replace part of the O atoms. To guarantee full relaxations for all the structure and adsorption of intermediates, we have applied 20 Å vacuum space in the z-axis for sufficient space. The convergence criteria of the geometry optimizations have been established as follows: (1) the Hellmann-Feynman forces on the atom should be less than 0.001 eV/Å, (2) the total energy difference should be less than 5×10^{-5} eV/atom, and (3) the inter-ionic displacement should be less than 0.005 Å.

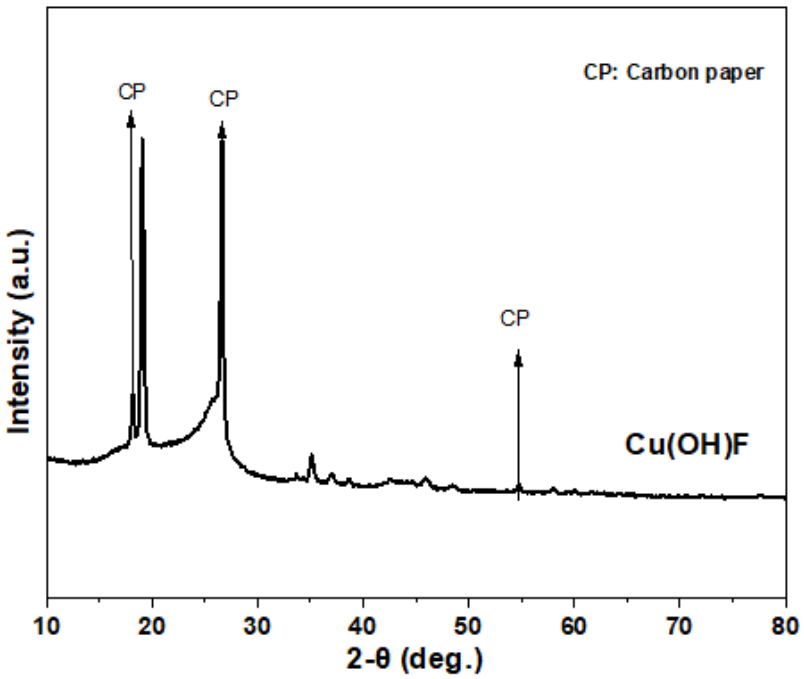

Figure S1. XRD pattern of Cu(OH)F precursor.

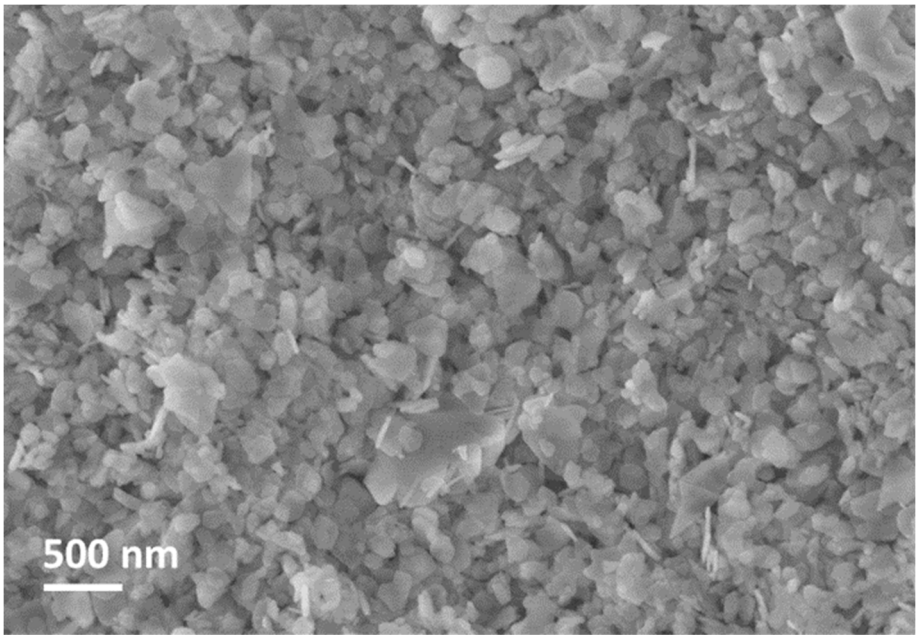

Figure S2. SEM image of Cu(OH)F precursor.

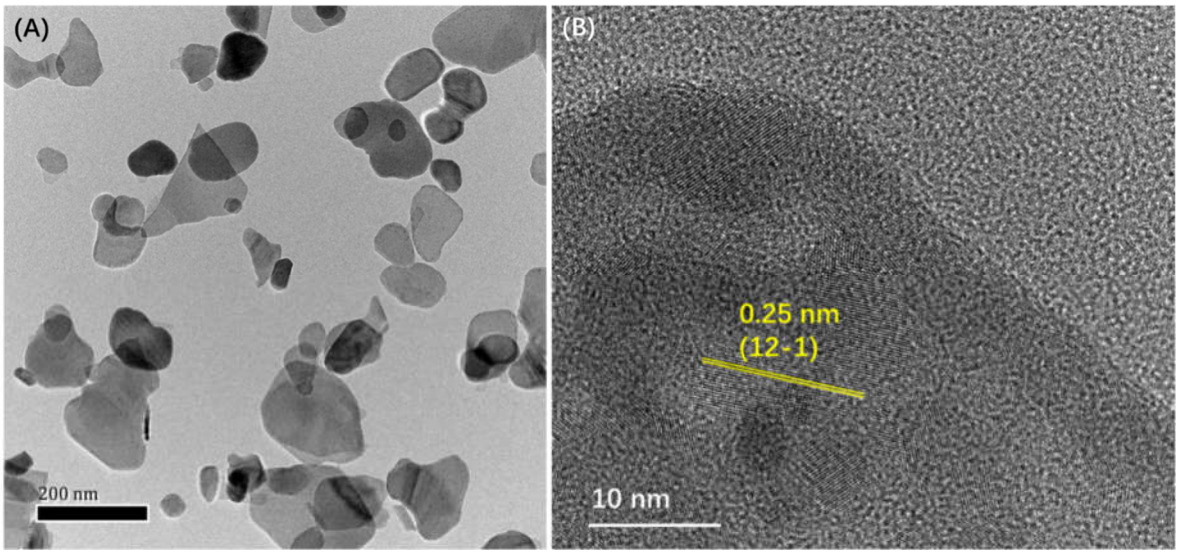

Figure S3. TEM (A) and HRTEM (B) images of Cu(OH)F precursor.

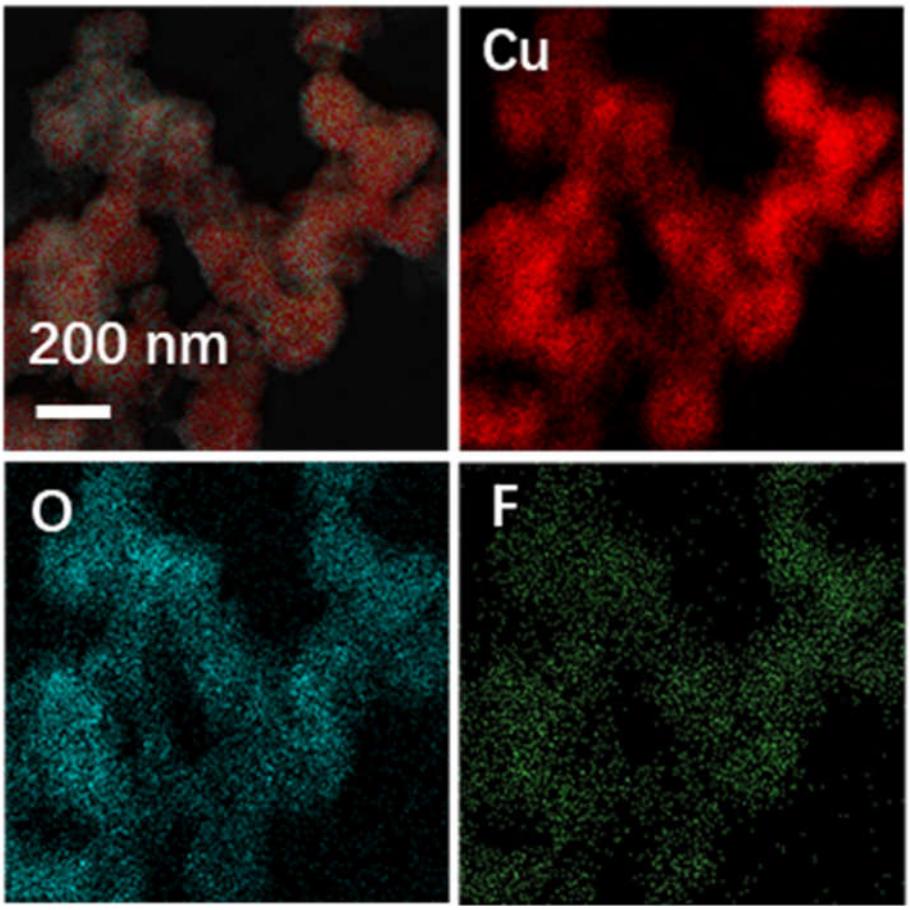

Figure S4. TEM-EDX of Cu/Cu_xOF derived from Cu(OH)F precursor.

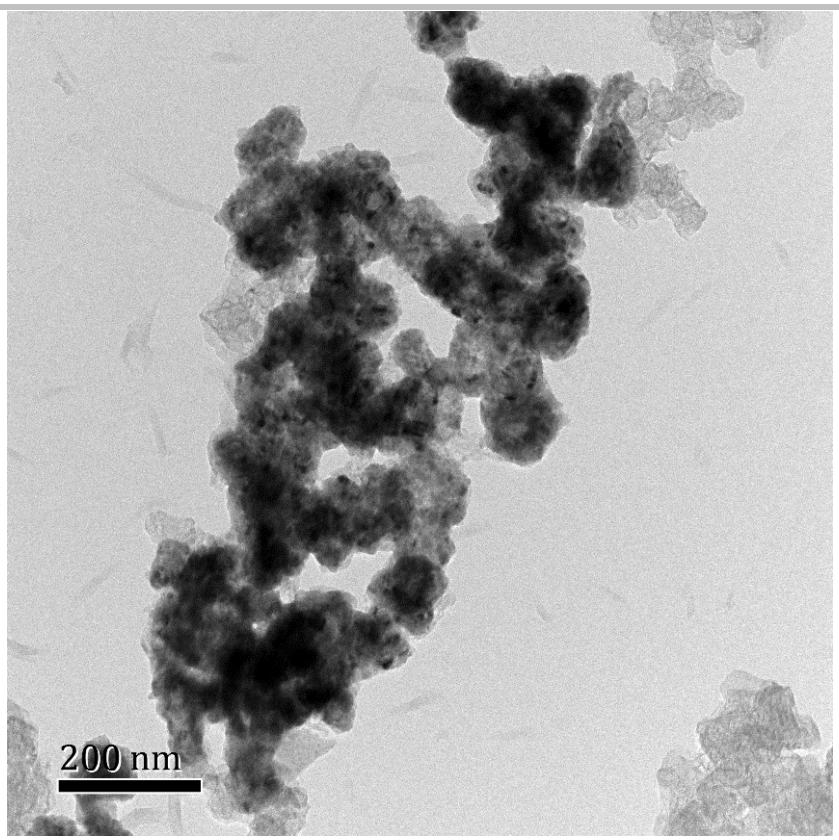

Figure S5. TEM image of Cu/Cu_xOF.

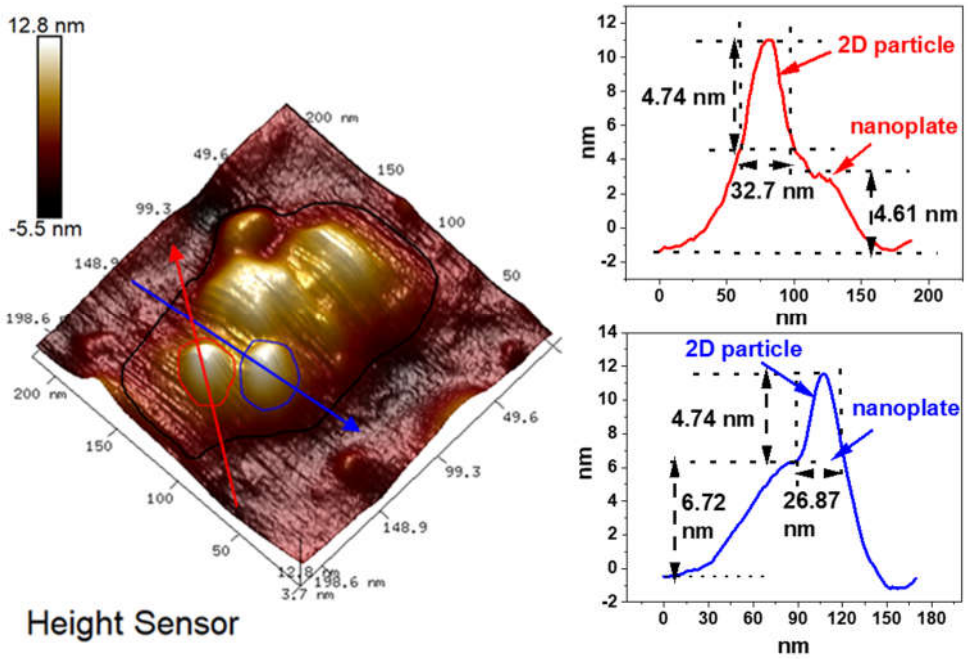

Figure S6. AFM image & corresponding height profiles of Cu/Cu_xOF showing the nanoplates and 2D particles.

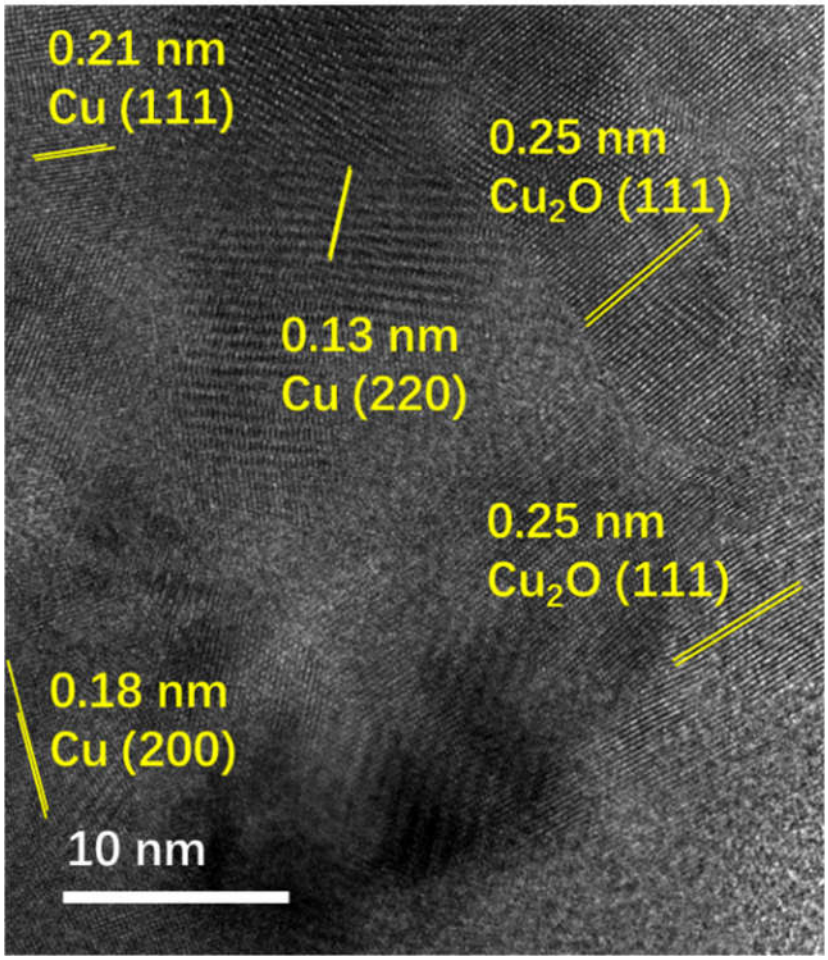

Figure S7. HRTEM image of Cu/Cu_xOF with lattice fringes that could be ascribed to Cu_2O (111), metallic Cu (111), (200) and (220).

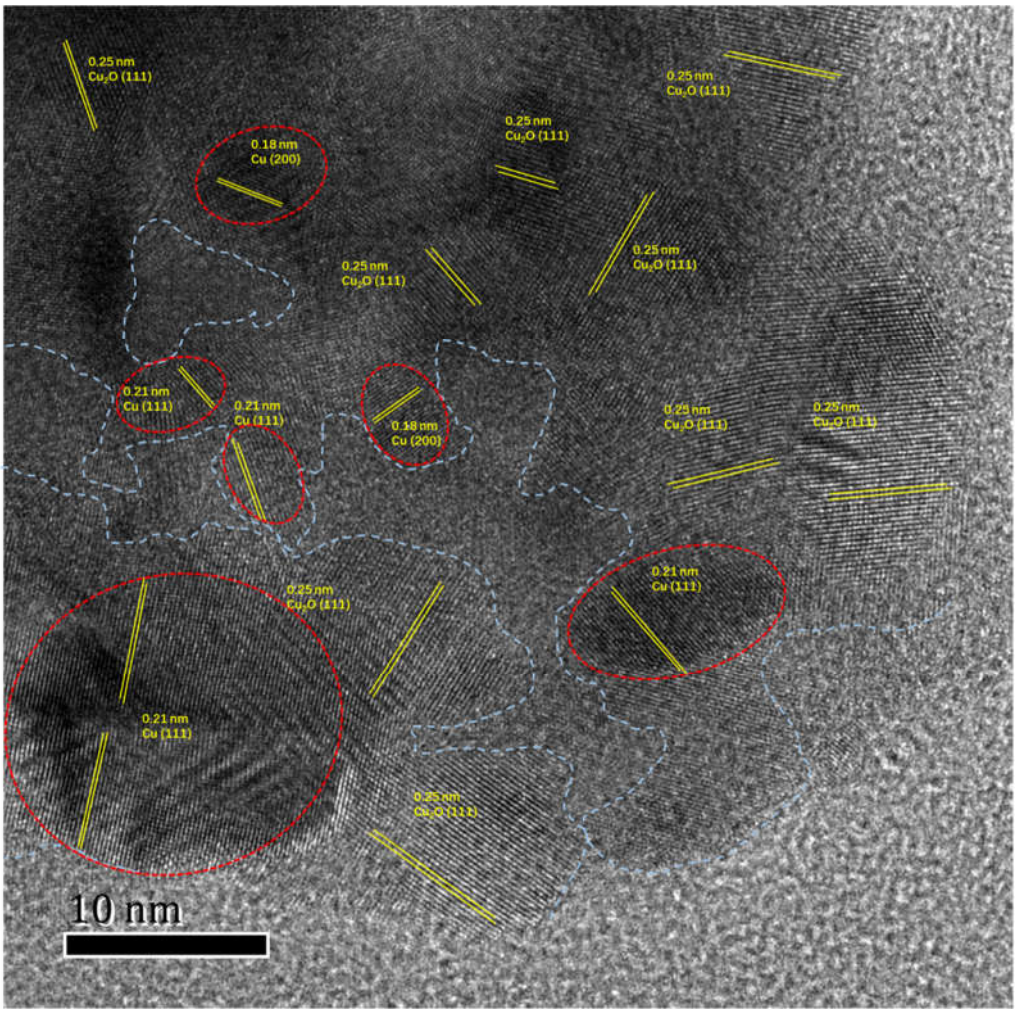

Figure S8. HRTEM image of Cu/Cu_xOF shows the well crystallized metallic Cu nanoparticles (red circles) as well as the crystallized Cu_2O and amorphous regions (blue dotted lines labeled regions) in Cu_xOF.

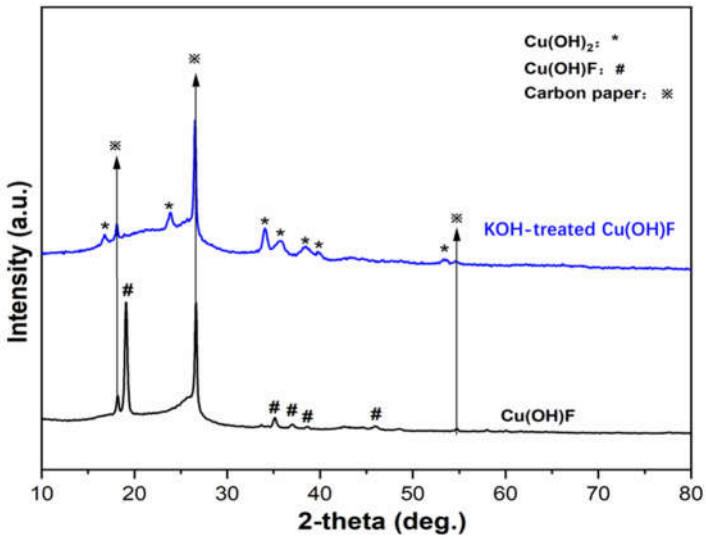

Figure S9. XRD spectra of Cu(OH)F and KOH-treated Cu(OH)F.

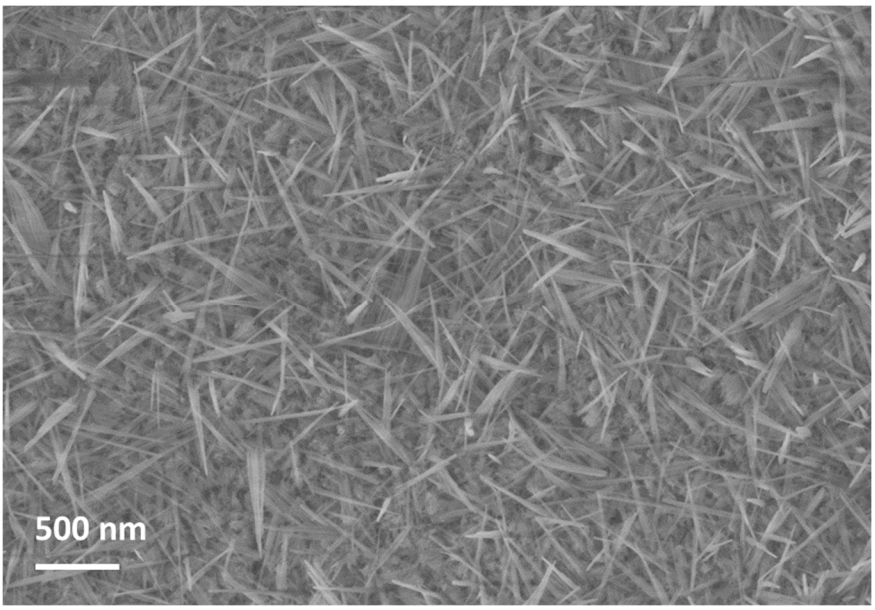

Figure S10. SEM image of KOH-treated Cu(OH)F.

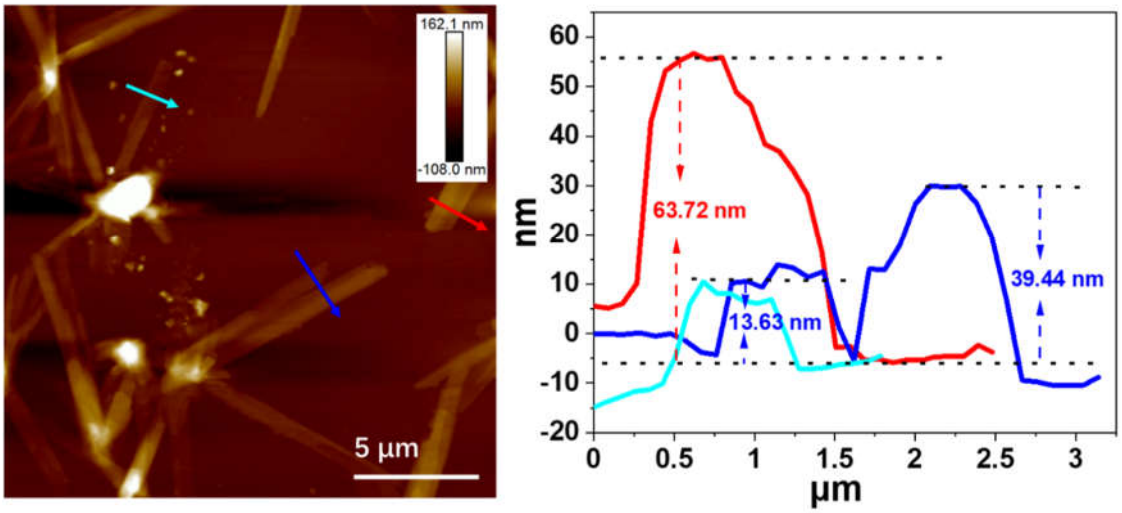

Figure S11. AFM image of KOH-treated Cu(OH)F.

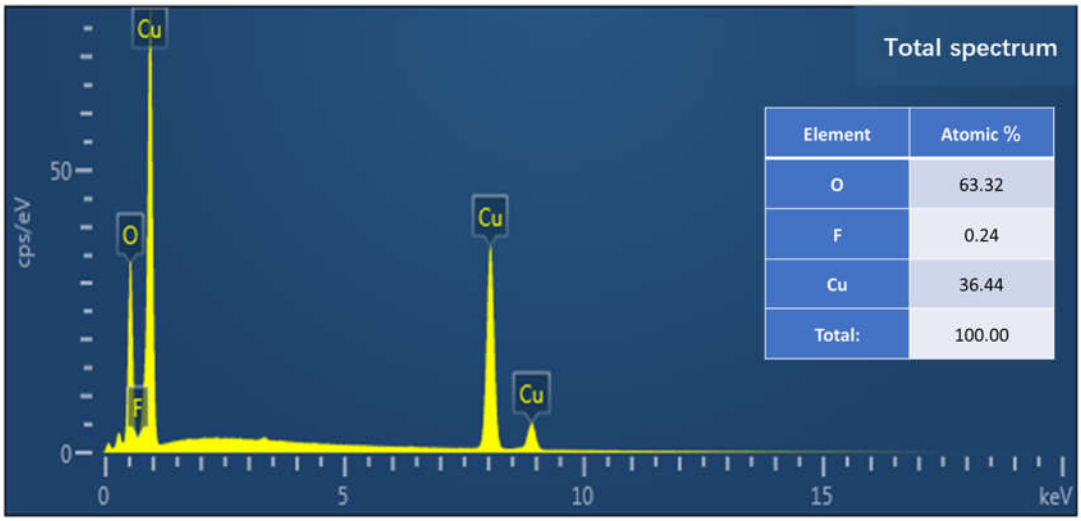

Figure S12. EDX spectrum of KOH-treated Cu(OH)F showing the concentration of F was greatly reduced to 0.24%.

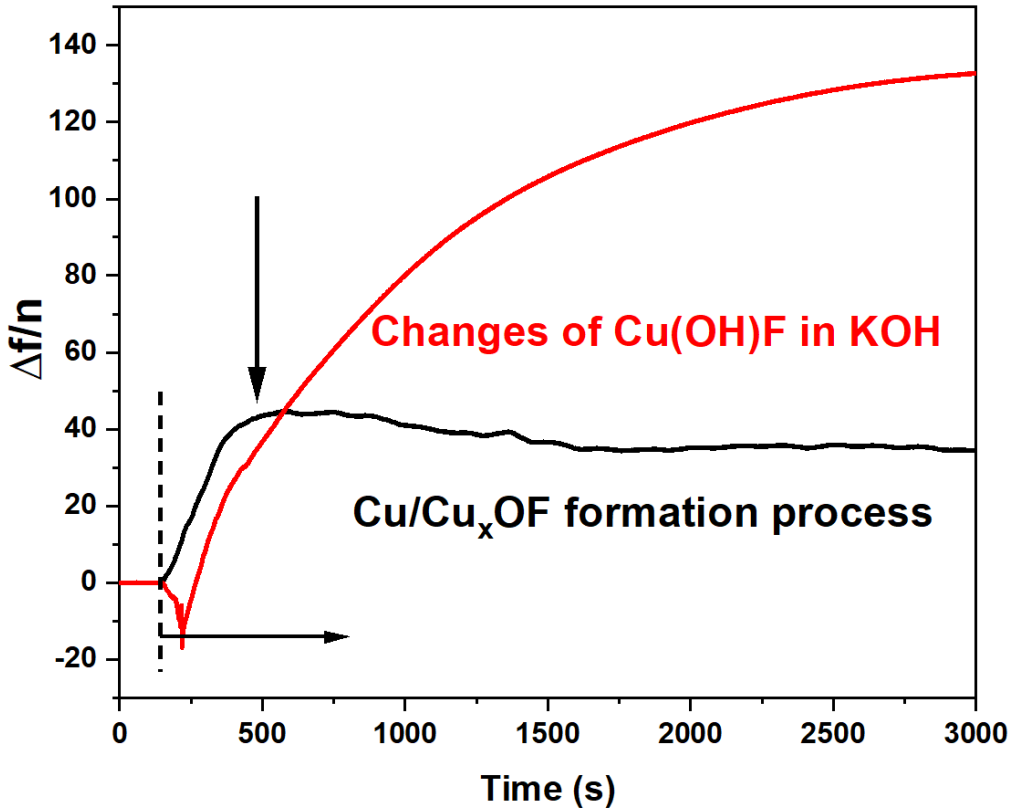

Figure S13. *In situ* EQCM-D that tracks the chemical- and electrochemical transformation processes of Cu(OH)F.

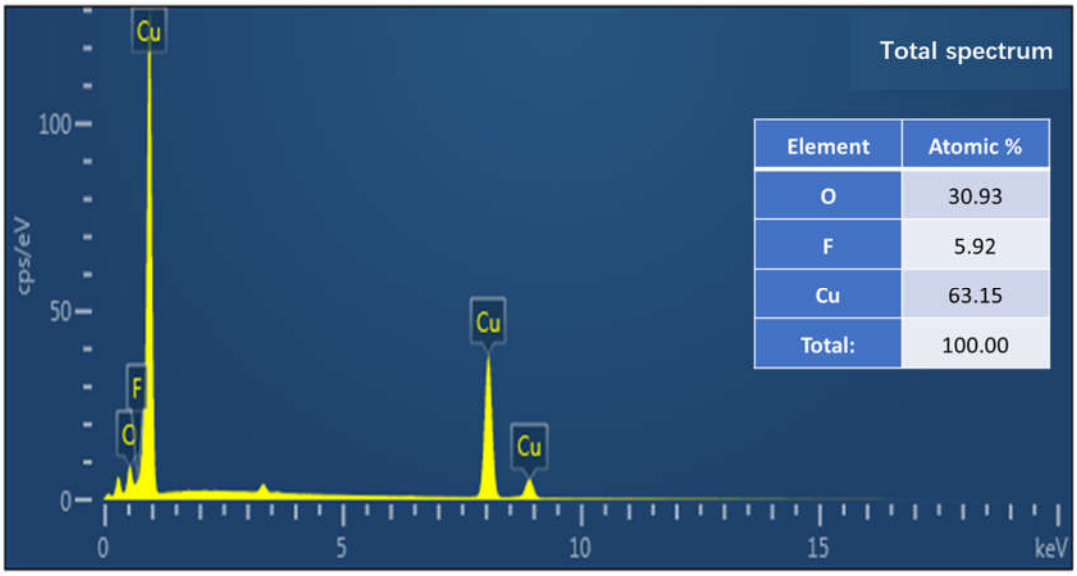

Figure S14. EDX spectrum of Cu/Cu_xOF derived from the electrochemical transformation of Cu(OH)F showing the concentration of F was 5.92%.

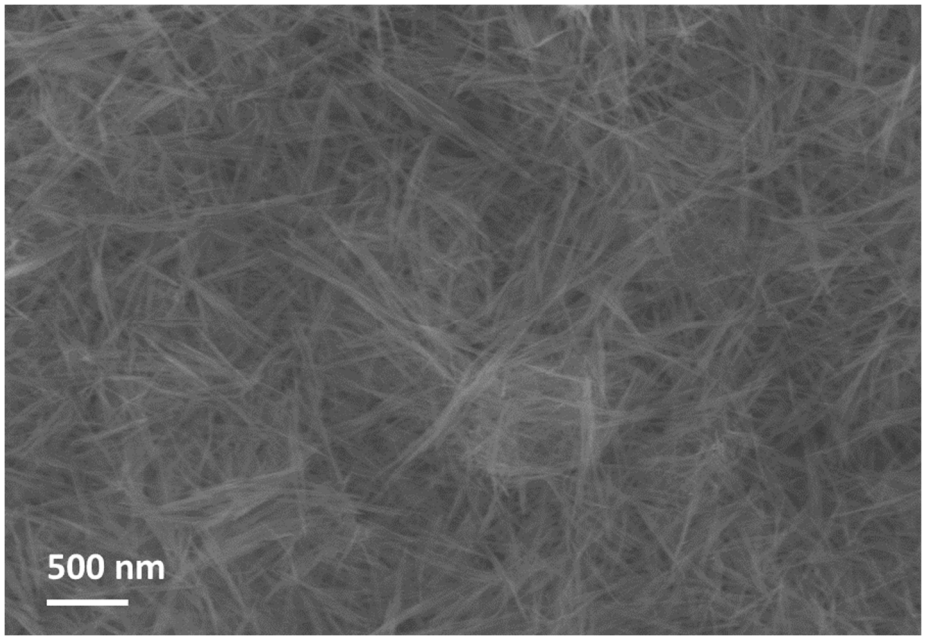

Figure S15. SEM image of $Cu(OH)_2$ precursor.

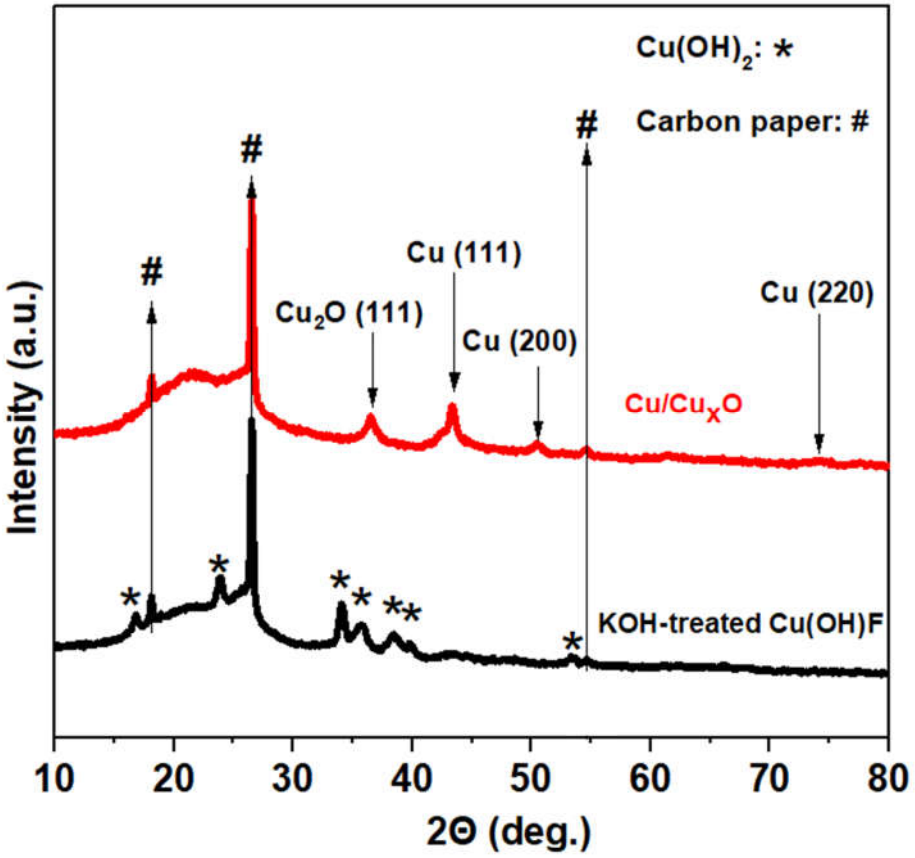

Figure S16. XRD pattern of KOH-treated Cu(OH)F (black curve) and Cu/Cu_xO (red curve).

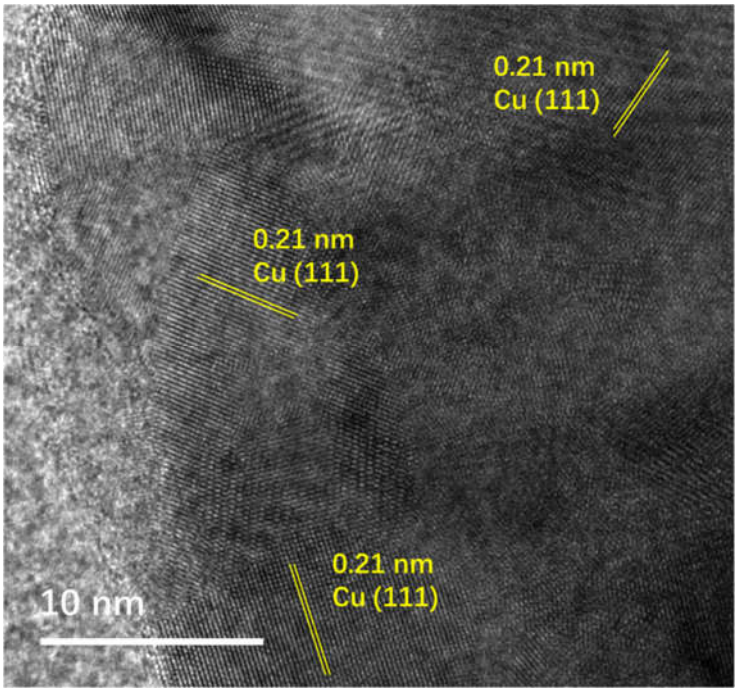

Figure S17. HRTEM image of Cu-(111) showing the lattice fringe of Cu (111) facet.

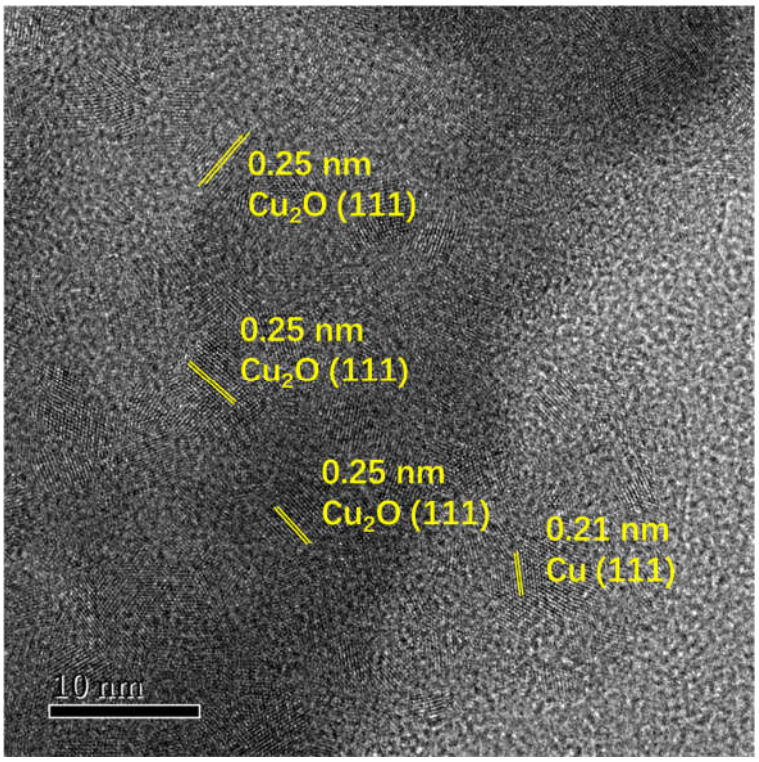

Figure S18. HRTEM image of Cu/Cu_xO.

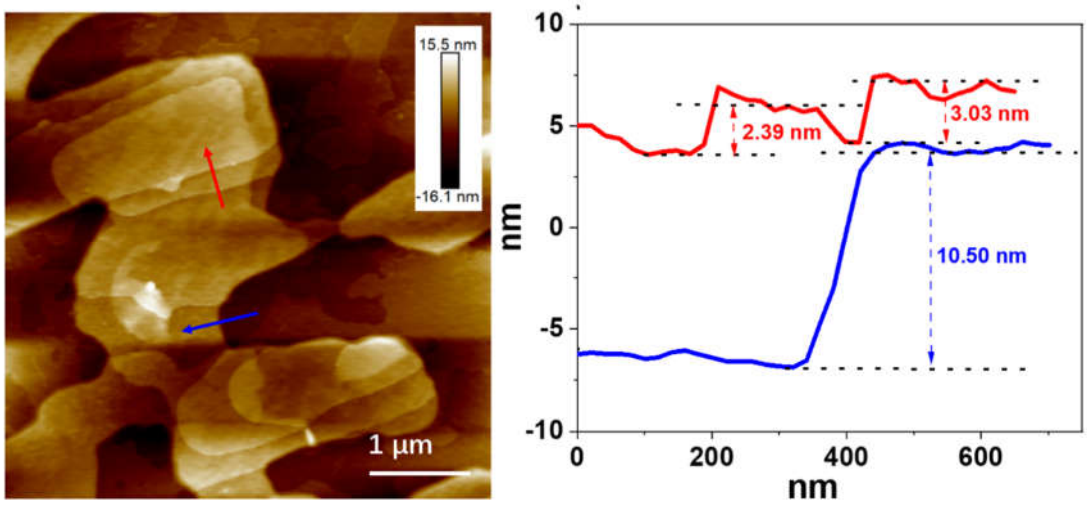

Figure S19. AFM image of Cu-(111) showing the 2D micro-structure with smooth surface.

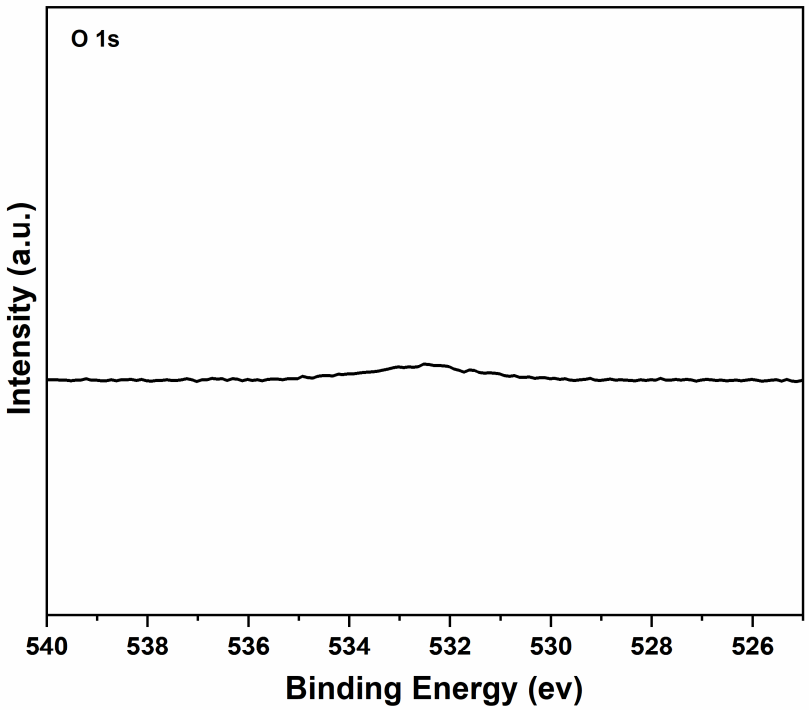

Figure S20. High resolution XPS spectrum of Cu-(111) at O 1s spin-orbital showing negligible peak.

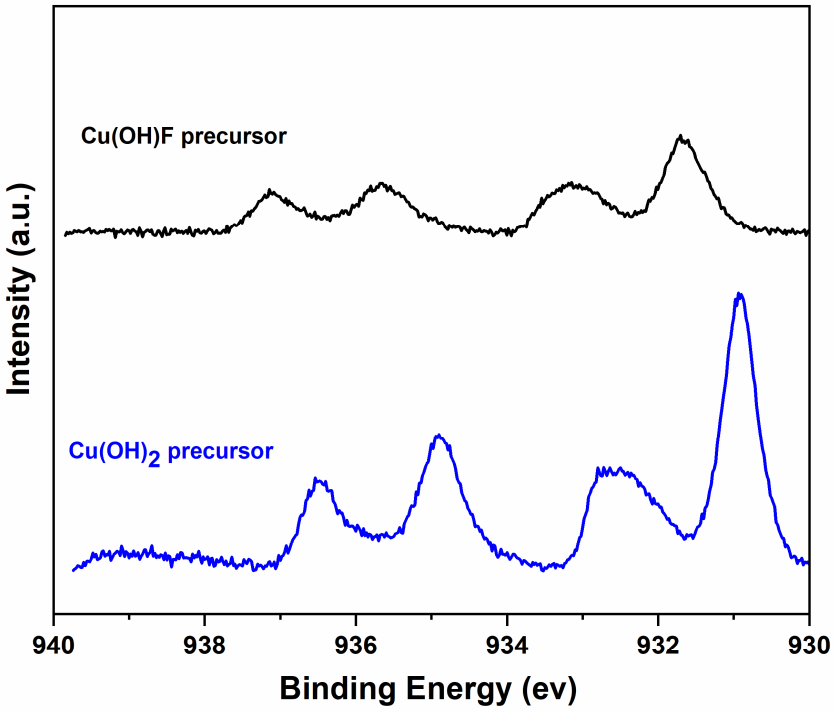

Figure S21. High resolution XPS spectra of $Cu(OH)_2$ and Cu(OH)F precursors in Cu 2p spin-orbital.

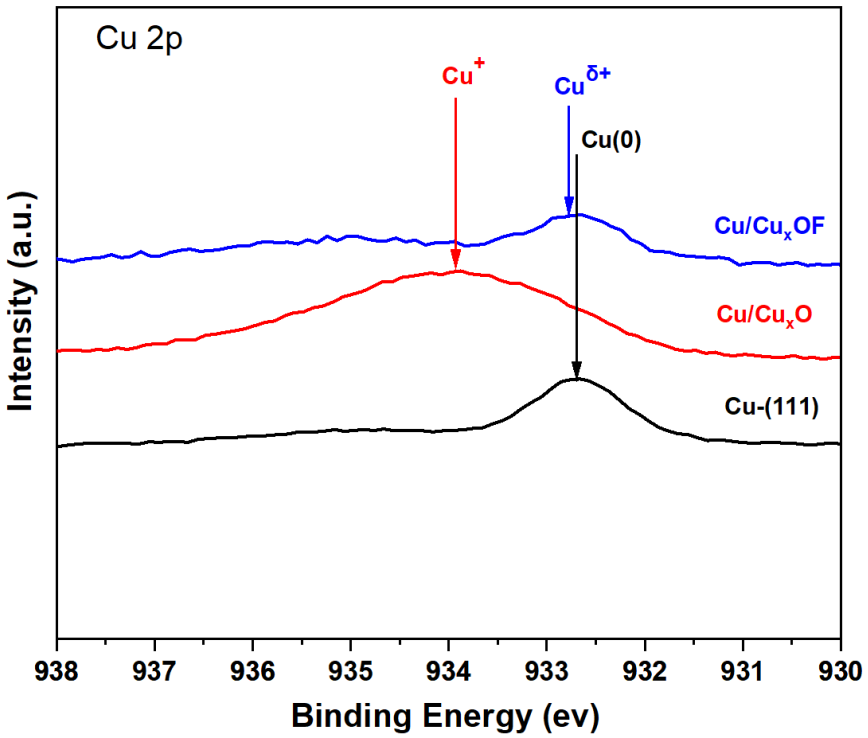

Figure S22. XPS spectra of Cu/Cu_xOF, Cu/Cu_xO and Cu-(111) derived from electrochemical transformation from Cu(OH)F, KOH-treated Cu(OH)F and $Cu(OH)_2$ precursors.

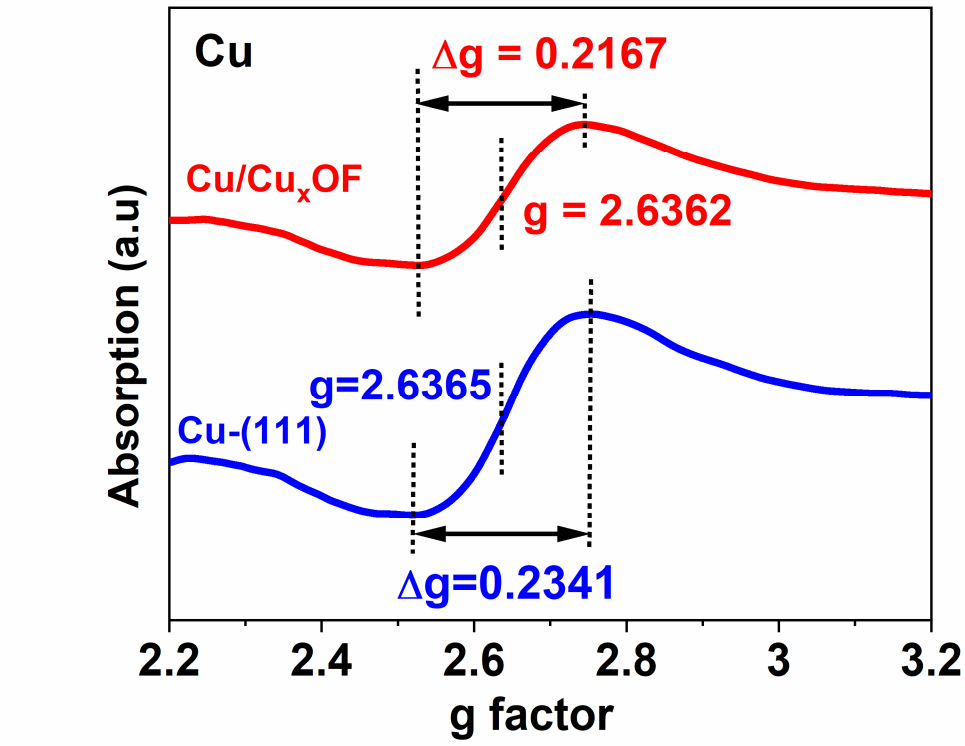

Figure S23. EPR spectra of Cu/Cu_xOF and Cu-(111) at Cu position.

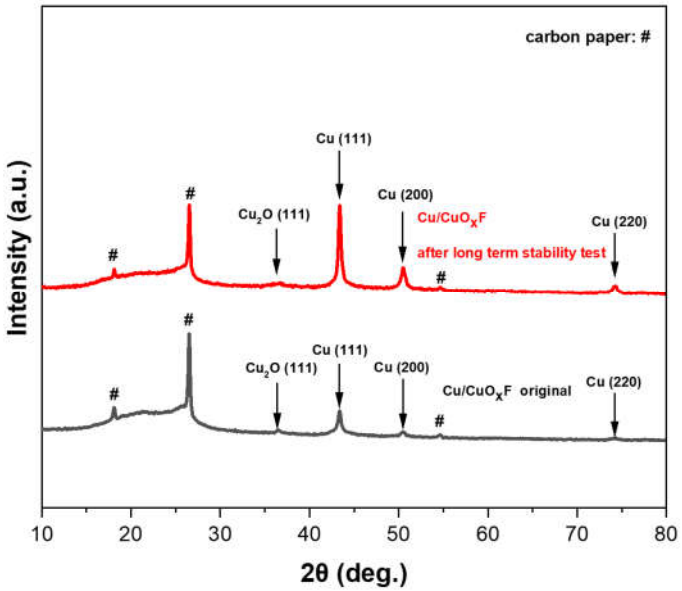

Figure S24. XRD of Cu/Cu$_x$OF after ~28 h stability test under the stepped potentials from -0.3 to -0.7 V vs RHE.

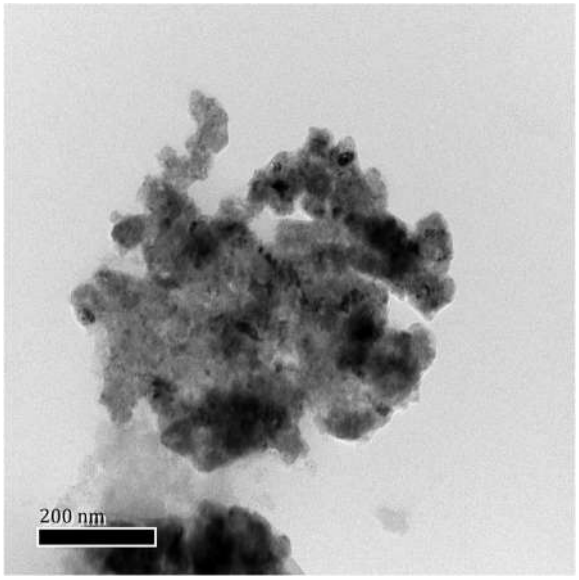

Figure S25. TEM image of Cu/Cu$_x$OF after ~28 h stability test under the stepped potentials from -0.3 to -0.7 V vs RHE.

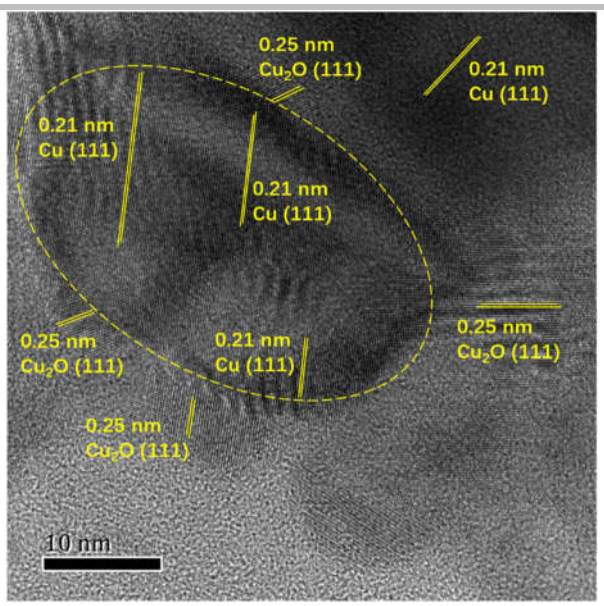

Figure S26. HRTEM image of Cu/Cu_xOF after ~28 h stability test under the stepped potentials from -0.3 to -0.7 V vs RHE.

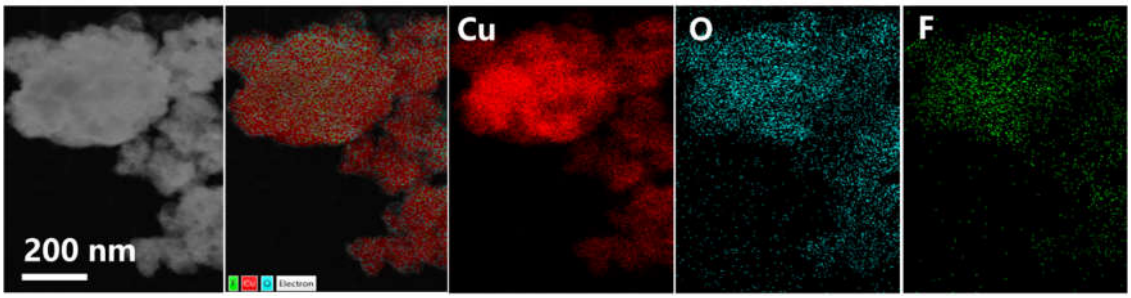

Figure S27. TEM-EDX mappings and corresponding spectrum of Cu/Cu_xOF after ~28 h stability test under the stepped potentials from -0.3 to -0.7 V vs RHE.

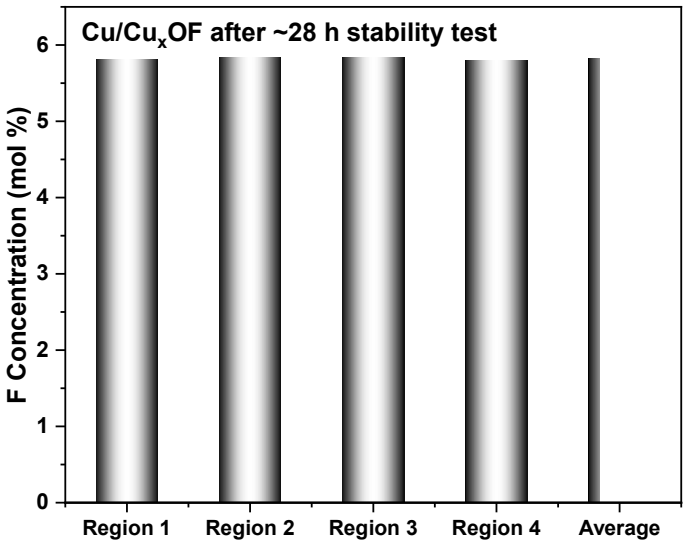

Figure S28. F concentration determined by EDX in 4 different points on Cu/Cu$_x$OF electrode after ~ 28 h stability test at the potential range from -0.3 V to -0.7 V *vs.* RHE.

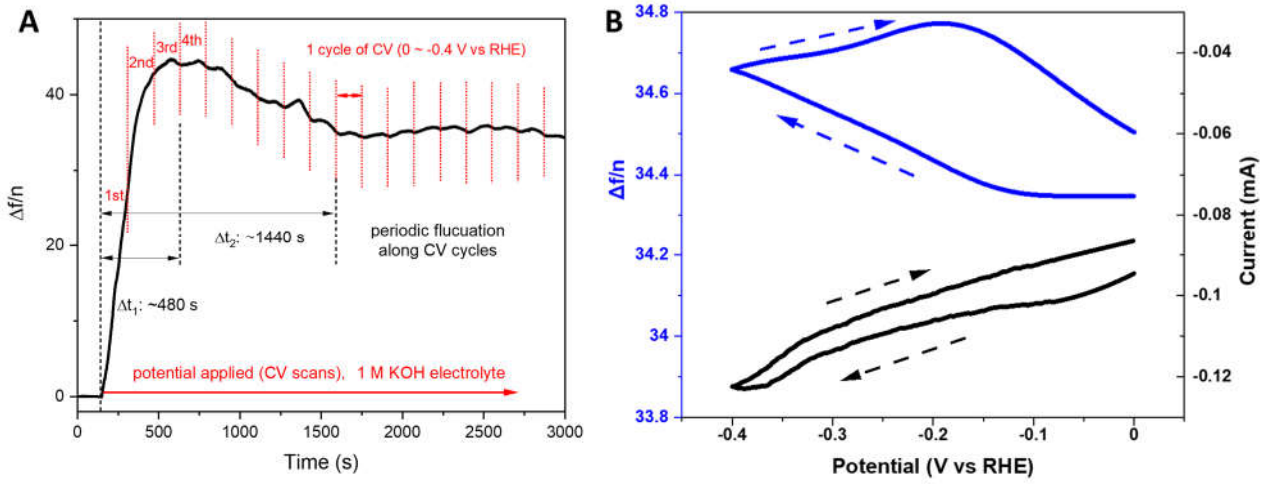

Figure S29. (A) *In situ* EQCM-D showing the periodic adsorption-desorption fluctuations along the CV cycles at the potential range of 0 ~ -0.4 V (vs RHE) in 1 M KOH, (B) variation of j/E curve (black) and Δf/n of a representative CV cycle (11th cycle) labeled in (A).

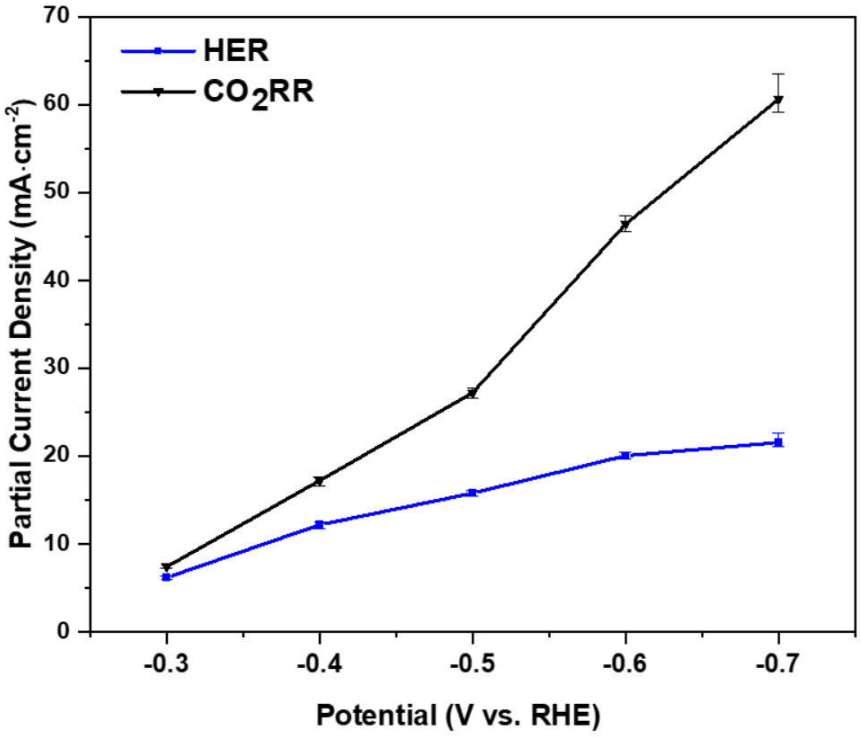

Figure S30. Partial current density of HER and CO_2RR on Cu/Cu_xOF.

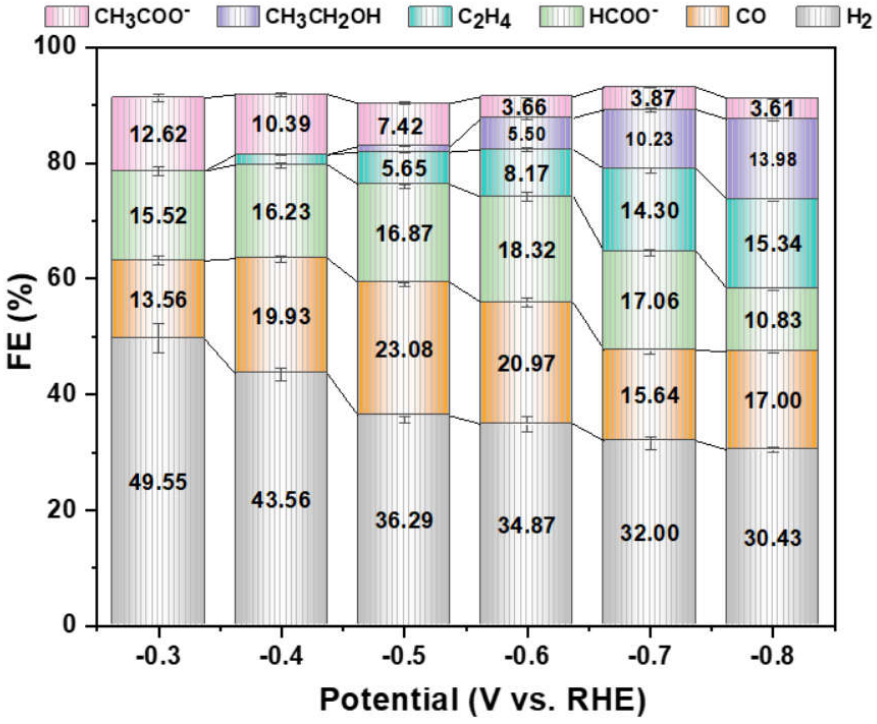

Figure S31. CO_2RR performance of Cu-(111) derived from $Cu(OH)_2$.

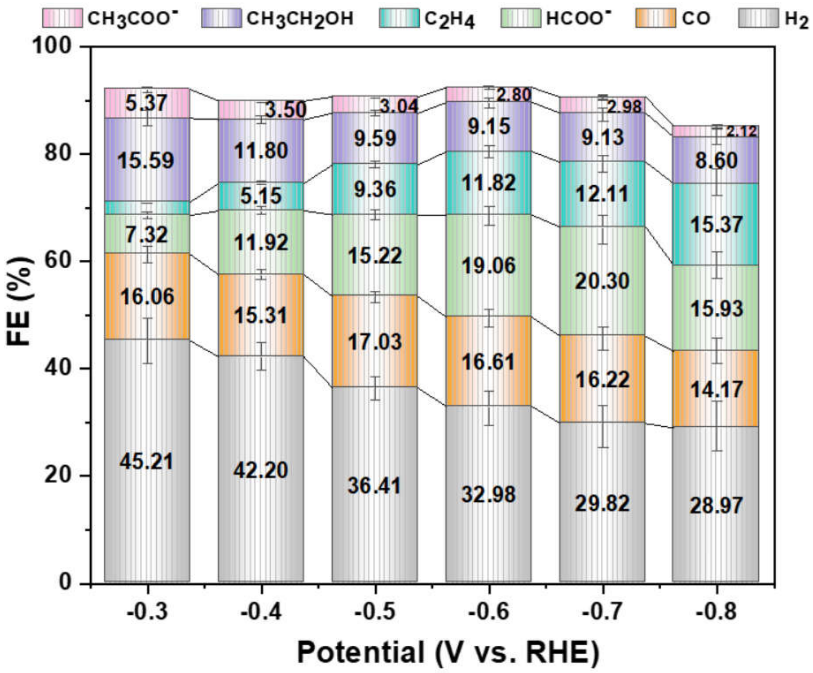

Figure S32. CO_2RR performance of Cu/Cu_xO hybrid made from KOH-treated Cu(OH)F.

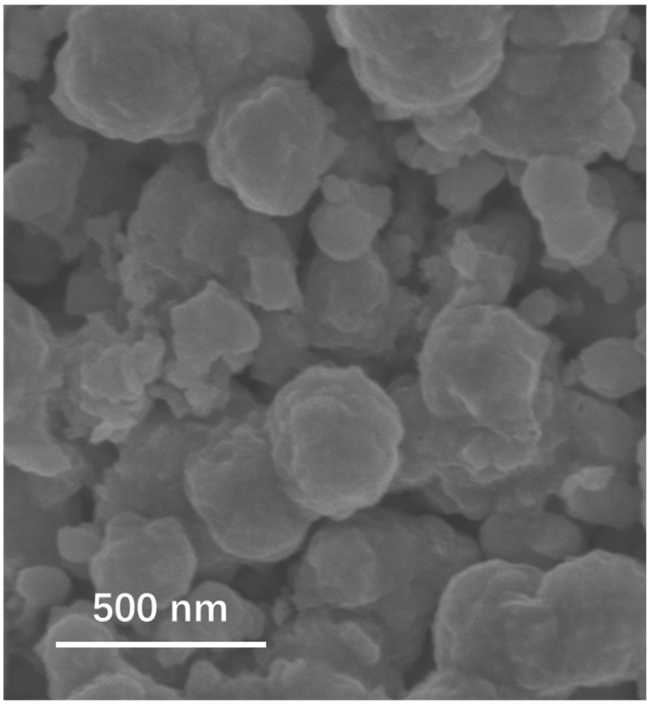

Figure S33. SEM image of Cu/Cu_xO derived from KOH-treated Cu(OH)F.

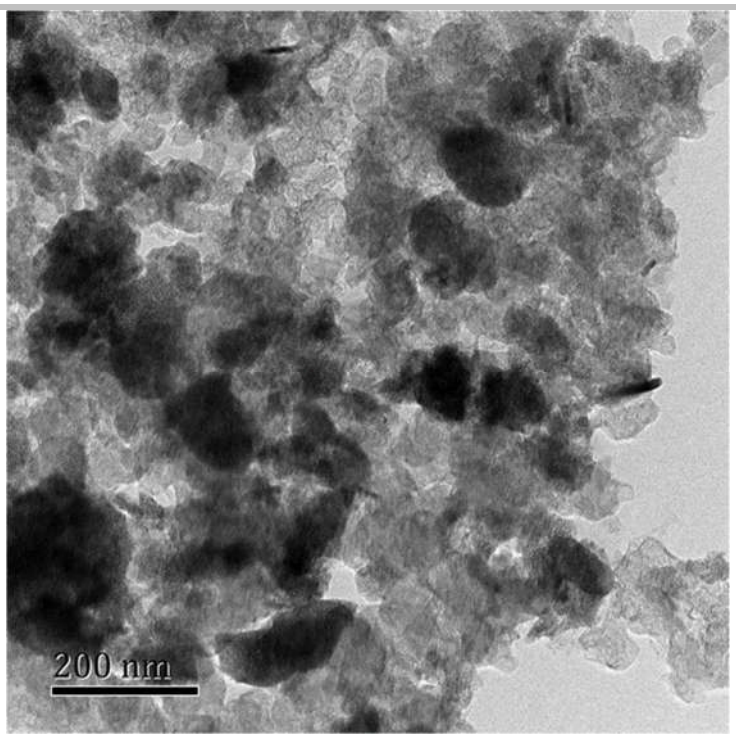

Figure S34. TEM image of Cu/Cu_xO.

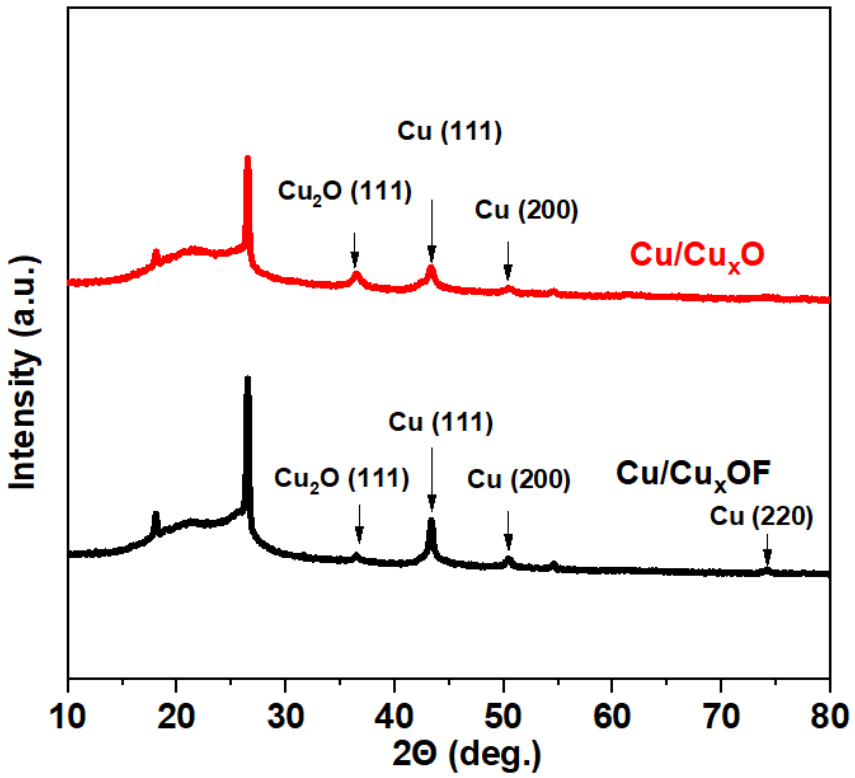

Figure S35. XRD spectra of Cu/Cu_xO (red curve) and Cu/Cu_xOF (black curve).

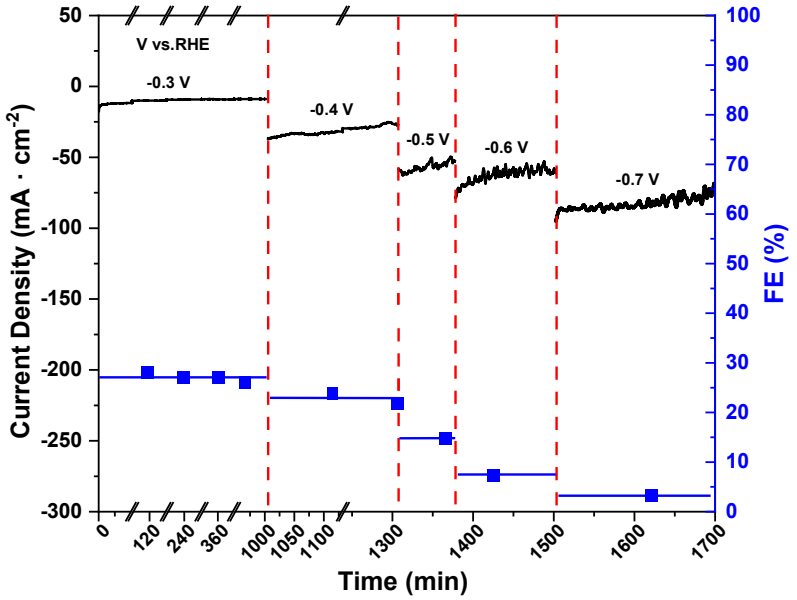

Figure S36. Stability tests on Cu/Cu_xOF and corresponding FE of CH_3COO^- under the potential range of -0.3 V ~ -0.7 V vs RHE. The evolution trend of FE was labeled with blue lines showing a stable selectivity for HER and acetate production on Cu/Cu_xOF.

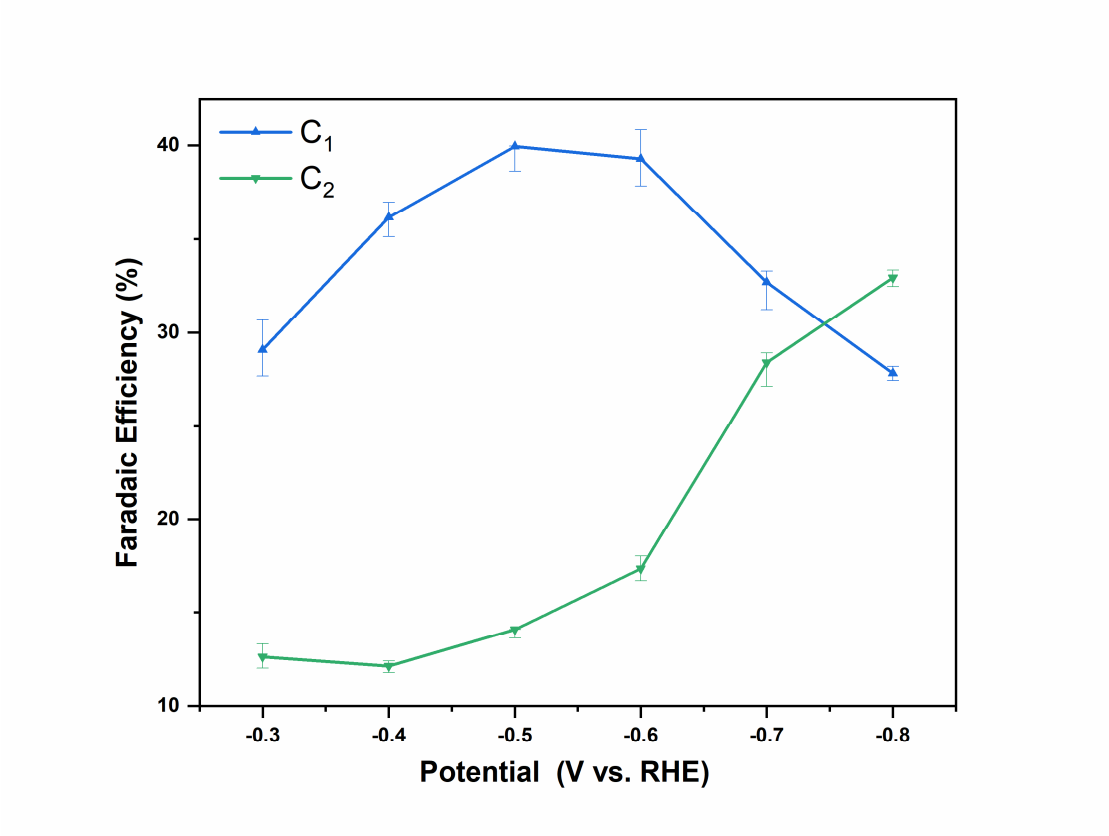

Figure S37. FE of C_2 and C_1 as the function of applied potentials on Cu-(111).

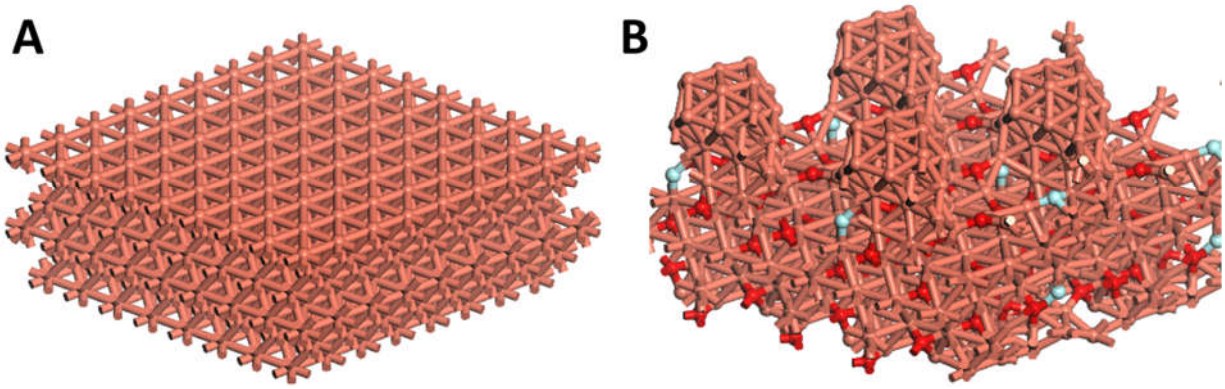

Figure S38. The relaxed structures of (A) Cu-(111) and (B) Cu/Cu_xOF. Orange balls = Cu, red balls = O, cyan balls = F.

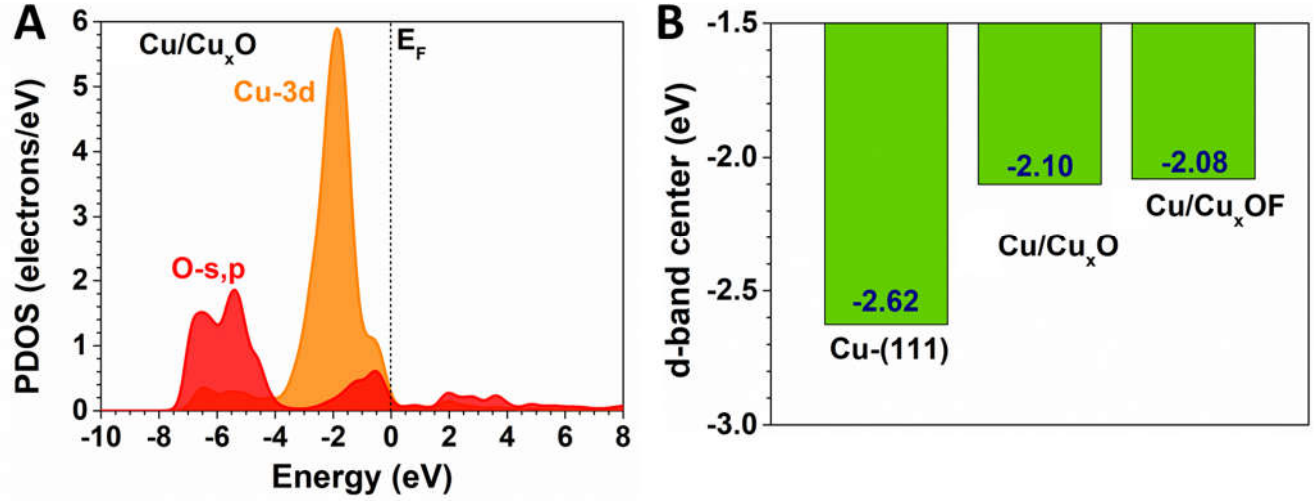

Figure S39. (A) The PDOS of Cu/Cu_xO and (B) the d-and center comparison among different samples.

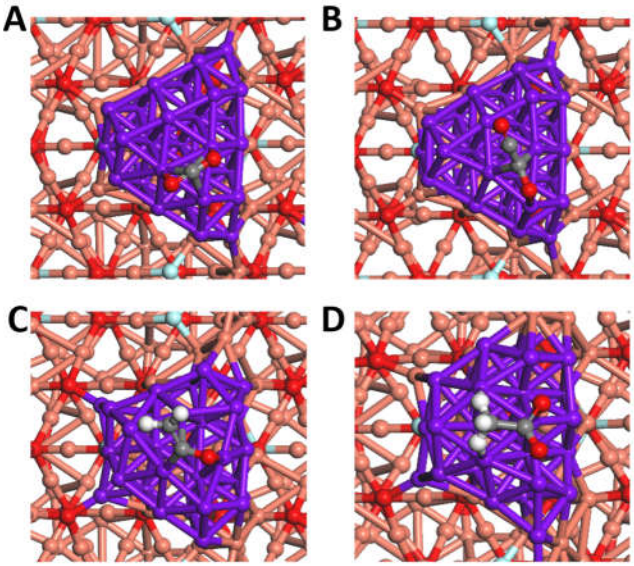

Figure S40. The structural configurations of key adsorbates of (a) CO_2, (b) OCCO, (c) CH_2CO and (d) CH_3COO^-. Orange balls = Cu in Cu_xOF, purple balls = H-Cu on the surface, red balls = O, cyan balls = F, grey balls = C and white balls = H.

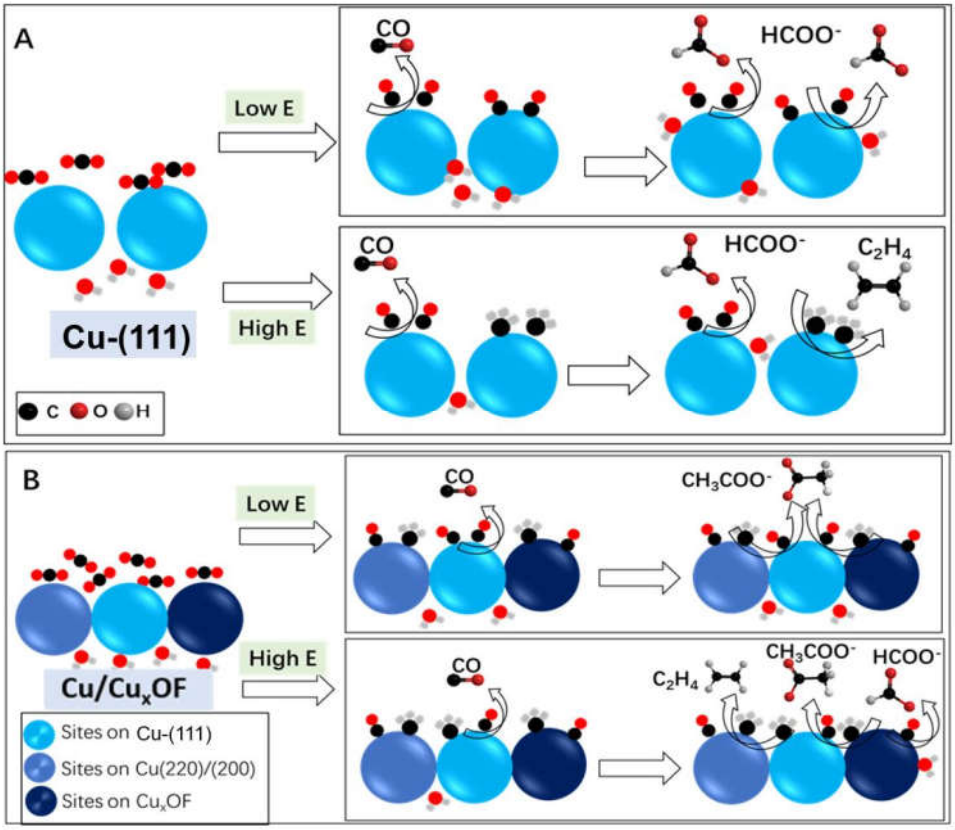

Scheme S1. Possible reaction pathways for CO_2 reduction towards various products on (A) Cu-(111) and (B) Cu/Cu_xOF at low and high overpotentials.

Tabel S1. Table of size statistics of Cu_XOF and Cu from well dispersed Cu/Cu_xOF

	Cu_xOF Nanoplate size		*Cu size*	
	Horizontal (nm)	Vertical (nm)	Horizontal (nm)	Vertical (nm)
1	~125	~4.61	~33	~4.74
2	~125	~6.72	~27	~4.74
3	~150	~3.44	~34	~2.29
4	~130	~6.16	~26	~2.66
5	~200	~8.40	~29	~2.36
6	~120	~8.86	~38	~5.16
7	~100	~6.68	~23	~2.12
8	~125	~6.02	~28	~5.04
Average	~134	~6.36	~30	~3.64

Table S2. Summary of the performance of the catalysts for CO_2RR towards the generation of acetic acid.

Reference	Catalysts	Potential (vs RHE) [V]	FE % (CH3COO-)	Current density [$mA \cdot cm^{-2}$]	Partial current density (CH3COO-) [$mA \cdot cm^{-2}$]	Electrolyte
Ref1[2]	Mn-corrole	−0.674	63.0	0.8	0.5	0.1 M phosphate buffer (pH 6)
Ref2[3]	Copper foil	-1.05	0.3	~ 8.0	~ 0.024	0.1 M KHCO3
Ref3[4]	Fe/N-C	−0.5 V vs Ag/AgCl (3 M KCl)	60.9	0.36	~ 0.219	0.05 M KHCO3
Ref4[5]	NDD/Si RA	-1.0	91.8	~ 0.76	~ 0.70	0.5 M $NaHCO_3$
Ref5[6]	$(Cu)_2$,$(Ag)_3$/ polymer/GCE films	-1.33	21.2	< 0.85	< 0.18	0.5 M KHCO3 with 8 ppm of benzotriazole
This work	Cu/Cu_xOF	-0.3	27.0	~14.5	~ 4.0	1 M KOH

Reference

[1] H. Tian, Y. Wang, J. Zhang, Y. Ma, H. Cui, Q. Cui, Y. Ma, *J. Phys. Chem. C* **2019**, *123*, 25492-25500.

[2] R. De, S. Gonglach, S. Paul, M. Haas, S. S. Sreejith, P. Gerschel, U.-P. Apfel, T. H. Vuong, J. Rabeah, S. Roy, W. Schöfberger, *Angew. Chem. Int. Ed.* **2020**, *59*, 10527-10534.

[3] K. P. Kuhl, E. R. Cave, D. N. Abram, T. F. Jaramillo, *Energy Environ. Sci.* **2012**, *5*, 7050-7059.

[4] C. Genovese, M. E. Schuster, E. K. Gibson, D. Gianolio, V. Posligua, R. Grau-Crespo, G. Cibin, P. P. Wells, D. Garai, V. Solokha, S. Krick Calderon, J. J. Velasco-Velez, C. Ampelli, S. Perathoner, G. Held, G. Centi, R. Arrigo, *Nat. Commun.* **2018**, *9*, 935.

[5] Y. Liu, S. Chen, X. Quan, H. Yu, *J. Am. Chem. Soc.* **2015**, *137*, 11631-11636.

[6] Y. Wang, D. Wang, C. J. Dares, S. L. Marquard, M. V. Sheridan, T. J. Meyer, *Proc. Natl. Acad. Sci. U.S.A.* **2018**, *115*, 278.

[7] S. J. Clark; M. D. Segall; C. J. Pickard; P. J. Hasnip; M. J. Probert; K. Refson; M. C. Payne, First Principles Methods Using Castep. *Zeitschrift Fur Kristallographie* **2005,** *220* (5-6), 567-570.

[8] J. P. Perdew; K. Burke; M. Ernzerhof, Generalized Gradient Approximation Made Simple. *Phys Rev Lett* **1996,** *77* (18), 3865-3868.

[9] P. J. Hasnip; C. J. Pickard, Electronic Energy Minimisation with Ultrasoft Pseudopotentials. *Comput Phys Commun* **2006,** *174* (1), 24-29.

[10] J. P. Perdew; J. A. Chevary; S. H. Vosko; K. A. Jackson; M. R. Pederson; D. J. Singh; C. Fiolhais, Atoms, Molecules, Solids, and Surfaces: Applications of the Generalized Gradient Approximation for Exchange and Correlation. *Physical Review B* **1992,** *46* (11), 6671-6687.

[11] J. D. Head; M. C. Zerner, A Broyden-Fletcher-Goldfarb-Shanno Optimization Procedure for Molecular Geometries. *Chem Phys Lett* **1985,** *122* (3), 264-270.